IJMMM International Journal of Minerals, Metallurgy and Materials 矿物冶金与材料学报（英文版）

Machine learning-assisted efficient design of Cu-based shape memory alloy with specific phase transition temperature

Mengwei Wu, Wei Yong, Cunqin Fu, Chunmei Ma, and Ruiping Liu

Cite this article as:
Mengwei Wu, Wei Yong, Cunqin Fu, Chunmei Ma, and Ruiping Liu, Machine learning-assisted efficient design of Cu-based shape memory alloy with specific phase transition temperature, *Int. J. Miner. Metall. Mater.*, 31(2024), No. 4, pp. 773-785. https://doi.org/10.1007/s12613-023-2767-6

View the article online at SpringerLink or IJMMM Webpage.

INTERNATIONAL JOURNAL OF
Minerals, Metallurgy and Materials

Volume 31, Number 4, April 2024
Page 773

Research Article https://doi.org/10.1007/s12613-023-2767-6

Machine learning-assisted efficient design of Cu-based shape memory alloy with specific phase transition temperature

Mengwei Wu[1),*], *Wei Yong*[2),*], *Cunqin Fu*[2)], *Chunmei Ma*[2),✉], *and Ruiping Liu*[1),✉]

1) Department of Materials Science and Engineering, China University of Mining & Technology (Beijing), Beijing 100083, China
2) Institute for Advanced Materials and Technology, University of Science and Technology Beijing, Beijing 100083, China
(Received: 8 June 2023; revised: 26 September 2023; accepted: 23 October 2023)

Abstract: The martensitic transformation temperature is the basis for the application of shape memory alloys (SMAs), and the ability to quickly and accurately predict the transformation temperature of SMAs has very important practical significance. In this work, machine learning (ML) methods were utilized to accelerate the search for shape memory alloys with targeted properties (phase transition temperature). A group of component data was selected to design shape memory alloys using reverse design method from numerous unexplored data. Component modeling and feature modeling were used to predict the phase transition temperature of the shape memory alloys. The experimental results of the shape memory alloys were obtained to verify the effectiveness of the support vector regression (SVR) model. The results show that the machine learning model can obtain target materials more efficiently and pertinently, and realize the accurate and rapid design of shape memory alloys with specific target phase transition temperature. On this basis, the relationship between phase transition temperature and material descriptors is analyzed, and it is proved that the key factors affecting the phase transition temperature of shape memory alloys are based on the strength of the bond energy between atoms. This work provides new ideas for the controllable design and performance optimization of Cu-based shape memory alloys.

Keywords: machine learning; support vector regression; shape memory alloys; martensitic transformation temperature

1. Introduction

Shape memory alloys (SMAs) are a new type of intelligent material based on martensitic transformation (MT) and reverse transformation, which has the characteristics of shape memory, superelasticity, damping performance, and vibration resistance [1–6]. In recent years, Cu-based SMAs have been widely used in military and civilian applications due to its low cost (only 1/10 of that of Ni–Ti alloy), excellent shape memory effect (SME), high superelasticity (SE), and good mechanical properties including executive components, heat protection components, pipe joints, environmental protection refrigerators, and energy conversion devices [7–12]. Most shape memory alloy-based devices are based on temperature-induced or stress-induced martensitic phase transformation. Therefore, the phase transformation temperature determines the temperature range used by the device and is the basis for the application of shape memory alloys.

The phase transition temperature of SMAs is very sensitive to the composition, and introducing elements to change the composition is the most commonly used method to adjust its high temperature or low temperature application. For example, Ni and Fe can increase the transition temperature of Cu–Al-based shape memory alloys, while Ti and Mn can reduce the transition temperature [13–17]. A small amount of alloying elements Ti, Mn, and Co can increase the transition temperature of Cu–Al–Ni SMAs, while Fe, Gr, and Nb will reduce the transformation temperature [18–19]. In many cases, the effect of the same element on the transformation temperature varies for different alloy systems, which add complexity to alloy design. Meanwhile, the addition of one alloying element leads to an exponential increase in the size and complexity of the alloy chemical search space. For Cu–Al based alloys, if the third element is added at 1wt%, the number of candidate alloy components can be as high as 10^6. It is difficult to experimentally search alloy compositions for specific phase transition conditions using traditional trial-and-error methods or first-principal calculations/density functional theory (DFT) methods. Therefore, it is crucial to explore an efficient and accurate method to search the complex composition space to reduce time and cost, and to predict the phase transition temperature quickly and accurately.

In recent years, the method based on combination of machine learning with low computing cost and short development cycle combined with powerful data processing and performance prediction has gradually entered the field of materials science and is widely used in characterization, analysis, and design of materials [20–24]. For example, Zhu *et al.*

*These authors contributed equally to this work.
✉ Corresponding authors: Chunmei Ma E-mail: haomerry@ustb.edu.cn; Ruiping Liu E-mail: lrp@cumtb.edu.cn

[25–26] successfully predicted the phase-forming ability, microstructure, and mechanical properties of high-entropy alloys (HEAs) through machine learning (ML), and realized the composition design of high-entropy alloys. Xue *et al*. [27–31] designed a systematic framework to effectively select the best combination of ML model and element features. Vecchio *et al*. [32] achieved successful prediction of crystal structure and solid solution forming ability by thermodynamic and chemical features with a random forest machine learning model. Yang *et al*. [33–35] utilized 13 descriptors of the ML model to predict solid solutions, intermetallic phases, and amorphous phases. Li *et al*. [36–37] proposed a new strategy to integrate the clustering formula method into three ML models to find β-phase-titanium alloys with low Young's modulus. Chou *et al*. [38] accelerated the discovery of low-modulus titanium alloys using the artificial neural network (ANN) method. Fu *et al*. [39–41] realized the performance-oriented composition design of high-performance copper alloys by optimizing the ML design system and built three random forest (RF) classifiers to accurately distinguish HEA phase formation. Tu *et al*. [42] compared various machine learning methods to search for the optimal configuration and design the magnetic-thermal properties of Mn–Fe–P–Si compounds. This approach accelerated the design and development process of excellent Mn–Fe–P–Si compounds. Rahaman *et al*. [43] discovered that on relatively small datasets, ensemble methods outperformed artificial neural networks. The above research demonstrates that utilizing cutting-edge algorithms, ML can establish quantitative relationships between material composition and performance, achieving effective and intelligent material composition design. Therefore, the use of machine learning methods is expected to solve the problem of quickly and accurately obtaining the alloy composition at a specific phase transition temperature in a huge search space, so as to realize the rational design and development of new Cu-based shape memory alloys.

This work explored a data-driven machine learning approach by using applied statistical tools to analyze the relationship between the transformation temperature of shape memory alloys and material descriptors (Cu-based SMAs elemental composition or alloying element features). In a wide range of Cu-based shape memory alloy compositions, this work reversed design alloy composition to achieve a specific phase transition temperature by both direct modeling of elemental composition and elemental feature modeling. By mapping the relationship between target properties and features, the mechanism of key features' influence on phase transition temperature was explored. This work will provide new ideas for the controllable design and performance optimization of Cu-based shape memory alloys.

2. Methodology

2.1. Alloy design framework

Two modeling methods were proposed to design shape memory alloys, including element composition modeling and element feature modeling, referred to as composition modeling and feature modeling. Design strategies for machine learning models for compositional modeling include: data collection→data collation→modeling→alloy design and experimental verification (Fig. 1). The model uses alloy element composition, heat treatment processing technology (temperature of heat-treatment (T_H), holding time of heat-treatment (t_H), quenching temperature (T_Q)), and differential scanning calorimetry (DSC) curve test heating/cooling rate (R_{DSC}) as input. Alloy martensitic transformation temperature (martensitic transformation finish temperature (M_f), martensitic transformation start temperature (M_s), austenite transformation start temperature (A_s), and austenite transformation finish temperature (A_f)) are used as output to establish composition-property relationship: (a) Data collection and feature extraction. Each data set consists of alloying element characteristics, heat treatment test process, and measured desired property (martensitic transformation temperature); (b) Feature screening. The correlation screening, recursive elimination, and exhaustive screening were used to screen the characteristics of alloy elements and obtain the most influential element characteristics of alloy properties; (c) Modeling and alloy prediction. Divide the collected data into training set data and testing set data, use the training data to learn feature-property relationships with associated uncertainties to predict the martensitic transformation temperature; (d) Alloy selection and experimental verification. Select candidate alloys in the unexplored compositional space based on empirical knowledge or performance requirements, measure the properties of candidate alloys through experiments, and compare the model prediction results with the experimental results to verify the model accuracy.

2.2. Data selection

A large number of relevant references were identified and obtained from the database, and the data of 76 Cu-based shape memory alloys were collected from the literature, including alloy composition, heat treatment process, phase transition temperature test conditions, and corresponding martensitic phase transition temperatures. The alloys of all data are processed under certain heat treatment conditions, and the specific element content and composition range are shown in Table 1.

2.3. Feature engineering

(1) Feature extraction.

According to the literature, the physical and chemical characteristics of elements, including atomic weight, melting temperature, electro-chemical factor, size factor, Mendeleev number, and lattice constants were extracted and classified.

(2) Feature screening.

The features extracted in the previous step were screened to select key features that have an important impact on the prediction model. The mean (f^i_{mean}) and standard deviation (f^i_{sd}) of alloy characteristics were calculated according to Eqs. (1)–(2). The f^i_{mean} and f^i_{sd} represent the average level

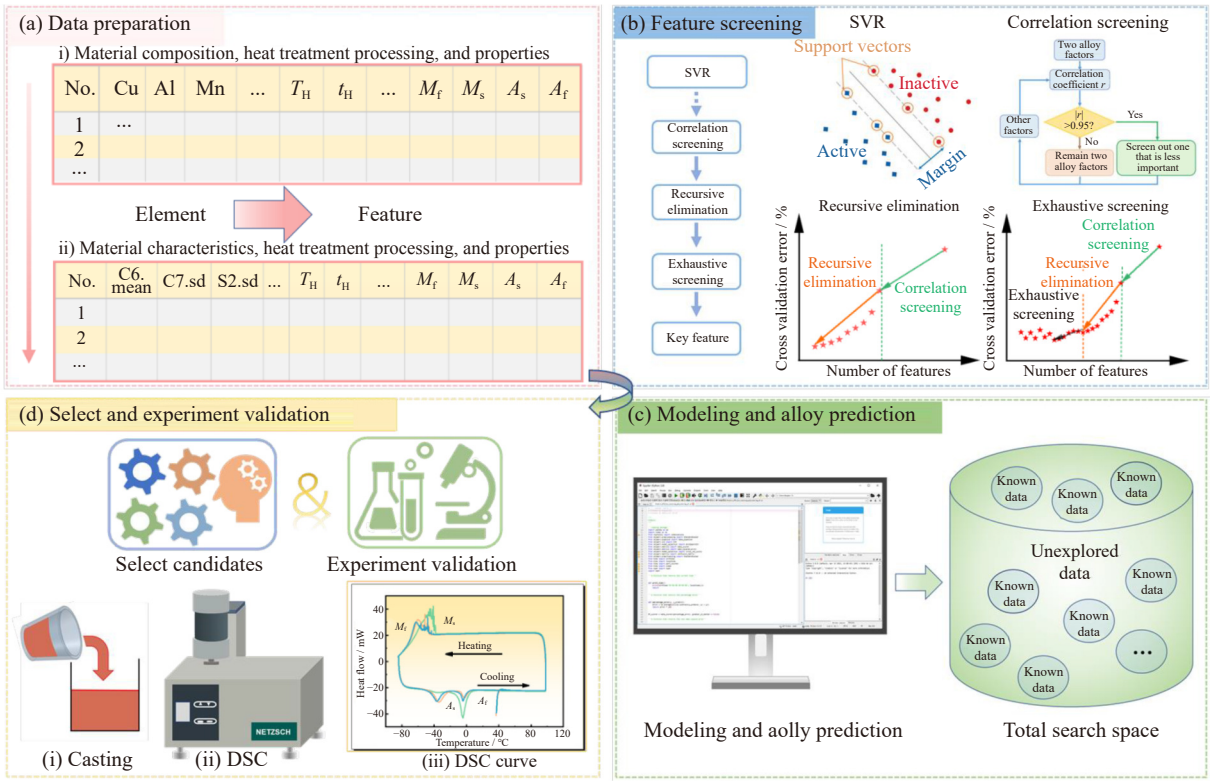

Fig. 1. Design framework of machine learning-assisted Cu-based shape memory alloy (SMAs) based on feature modeling.

Table 1. Alloy parameters in dataset

Alloy elements composition / at%								Heat treatment processing parameters			
Cu	Al	Ni	Ti	Mn	Co	Fe	Gd	T_H / K	t_H / min	T_Q / K	R_{DSC} / (K·min^{-1})
65.58–82.2	13.15–26.08	0–4.24	0–1.14	0–11.2	0–1.1	0–5.5	0–4.7	1073–1273	10–1440	–20/0/20	5–45

and fluctuation range of element feature values, respectively.

$$f^i_{\text{mean}} = \frac{\sum_{j=1}^{n} f^i_j \times \alpha_j}{\sum_{j=1}^{n} \alpha_j} \tag{1}$$

$$f^i_{\text{sd}} = \sqrt{\frac{\sum_{j=1}^{n} \left(f^i_j - f^i_{\text{mean}}\right)^2 \times \alpha_j}{\sum_{j=1}^{n} \alpha_j}} \tag{2}$$

where f^i_{mean} and f^i_{sd} are alloy factors; f^i_j is alloy elements and their physical–chemical characteristics, respectively; i and j are the i-th feature of the element and the j-th element of the alloy, respectively; α_j represents the atomic percent content of an element.

f^i_{mean} and f^i_{sd} are used as input, and correlation screening, recursive elimination [44], and exhaustive screening [45] are used to screen the key alloy factors that have the greatest influence on the alloy phase transition temperature. First, redundant features are quickly removed by correlation screening. Pearson correlation coefficient (r) between two alloying factors x and y are calculated according to Eq. (3).

$$r = \frac{\sum [(x_k - x_m) \times (y_k - y_m)]}{\sqrt{\sum (x_k - x_m)^2} \sqrt{\sum (y_k - y_m)^2}} \tag{3}$$

where x_k and y_k are the value of the two alloying factors in the k-th alloy (k = 1, 2,…, n), and x_m and y_m are the average values of these two alloying factors in 76 alloys.

The absolute value of the Pearson correlation coefficient ($|r| > 0.95$) indicates a strong linear correlation between the two alloy factors x and y, which means that they carry the same or similar information and thus have the same or similar influence on the alloy properties [46]. By using these two alloying factors as input to build a model, the alloying factor that has a large impact on the model error is eliminated, and only the factor that has a small impact on the model error is retained. The recursive elimination method is used to select one of the n features in turn, and the remaining n – 1 features are used as input to establish a regression model. Then, the alloy factor n corresponding to the minimum model error is removed, and n – 1 alloy factors that minimize the model error are retained. The elimination is recursively performed until the minimum model error changes from a downtrend to an uptrend. Finally, exhaustive screening is adopted, and all possible combinations of the remaining features after screening are used as input to establish prediction models respectively. Model errors are compared to identify key alloying factors or subsets that have the most significant impact on alloy properties.

2.4. Modeling

This work is to understand the quantitative relationship between the material properties (Y, transition temperature)

and the characteristics (X) of the material, that is, $Y = f(X)$. These methods determine how the response martensitic transformation temperature varies with alloy composition and key alloying factors. f is estimated using the support vector regression (SVR) method based on the radial basis function as the kernel function. Two hyperparameters of SVR, cost of making mistakes and gamma controlling the shape of the segmented hyperplane, are optimized using 10-fold cross-validation method. Taking the elemental composition and elemental key alloying factors as input, the relationship or mathematical model of elemental composition, elemental characteristics, and martensitic transformation temperature is established. The model error is determined by averaging the errors over the 10 validation datasets according to Eq. (4).

$$d = \frac{1}{n}\sum \frac{\left|P_{x\text{-predict}} - P_{x\text{-experiment}}\right|}{P_{x\text{-experiment}}} \times 100\% \quad (4)$$

where d is the error, $P_{x\text{-predict}}$ and $P_{x\text{-experiment}}$ are the predicted and measured characteristics, respectively [47].

2.5. Alloy prediction

The machine learning (ML) method described above makes accurate predictions of the target properties, i.e., transformation temperature (M_f, M_s, A_s, and A_f) for all unexplored data, as well as understanding how the transformation temperature (M_f, M_s, A_s, and A_f) is influenced by the alloy composition and key alloying factors. 61 sets of data are randomly selected from 76 sets of sample data for training, and the remaining 15 sets of data are used for testing.

2.6. Selection of alloy candidate and validation

To verify the accuracy of the model prediction, a group of alloy compositions ($Cu_{80.52}Al_{8.68}Mn_{10.8}$, wt%) with the room temperature phase transition temperature was selected in the unexplored range based on empirical knowledge and the application temperature range of the samples. Pure copper (99.9wt%), pure aluminum (99.9wt%), pure manganese (99.9wt%), and electrolytic nickel (99.5wt%) were used as raw materials, a cylindrical alloy with a diameter of ϕ60 mm was prepared by vacuum induction melting in an argon atmosphere. Then, the ingot was subjected to water quenching at 1123 K for 300 min. The transformation temperature (M_f, M_s, A_s, and A_f) of the exothermic/endothermic peaks were measured by DSC at a cooling/heating rate of 10 K·min^{-1}.

3. Results

The direct modeling of composition based on the cross-validation strategy has satisfactory prediction accuracy, as shown in Fig. 2. Modeling prediction results show that the errors of the training set and testing set of all composition-martensitic phase transformation models are below 4.5%.

Fig. 3 shows the correlation coefficient of 58 alloy factors with strong correlation. After correlation screening, 25 alloy

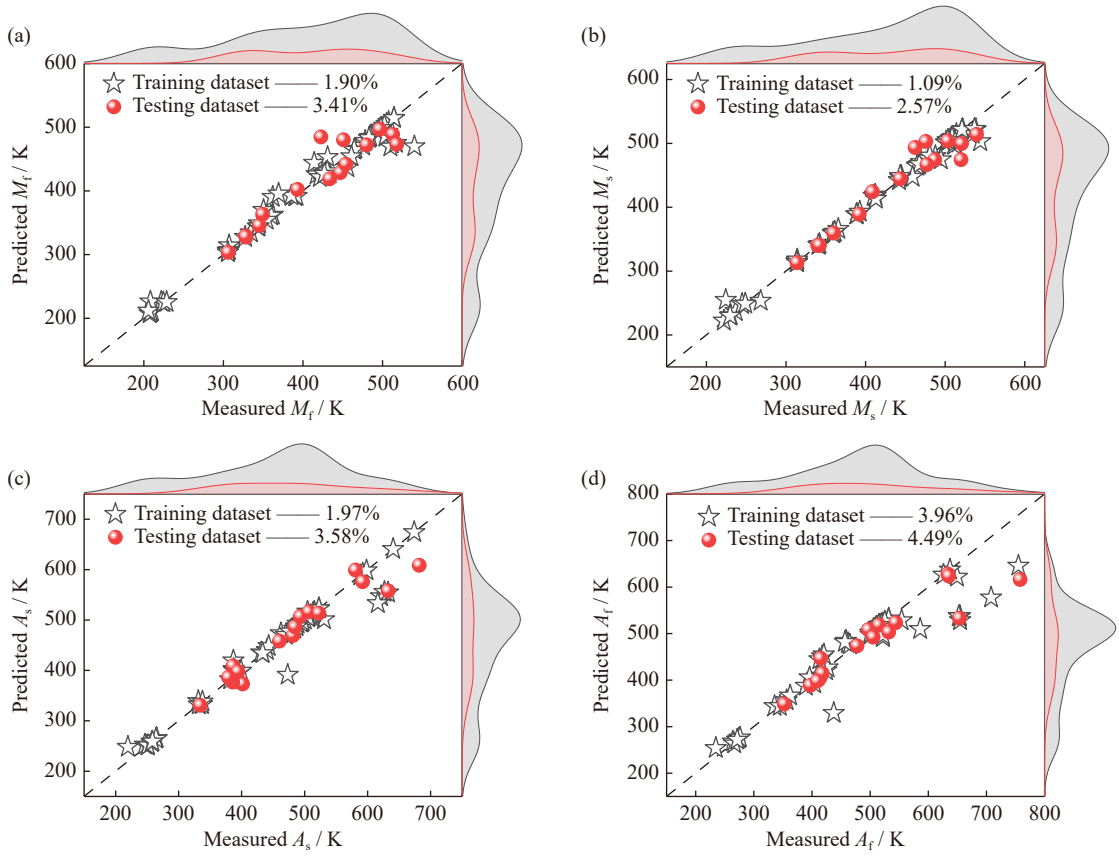

Fig. 2. Prediction results of component direct modeling: (a) predict error of component–M_f model; (b) predict error of component–M_s model; (c) predict error of component–A_s model; (d) predict error of component–A_f model. The shaded areas represent data distribution plots for the X and Y axes, offering more convenient and visual depiction of the data distribution on both axes.

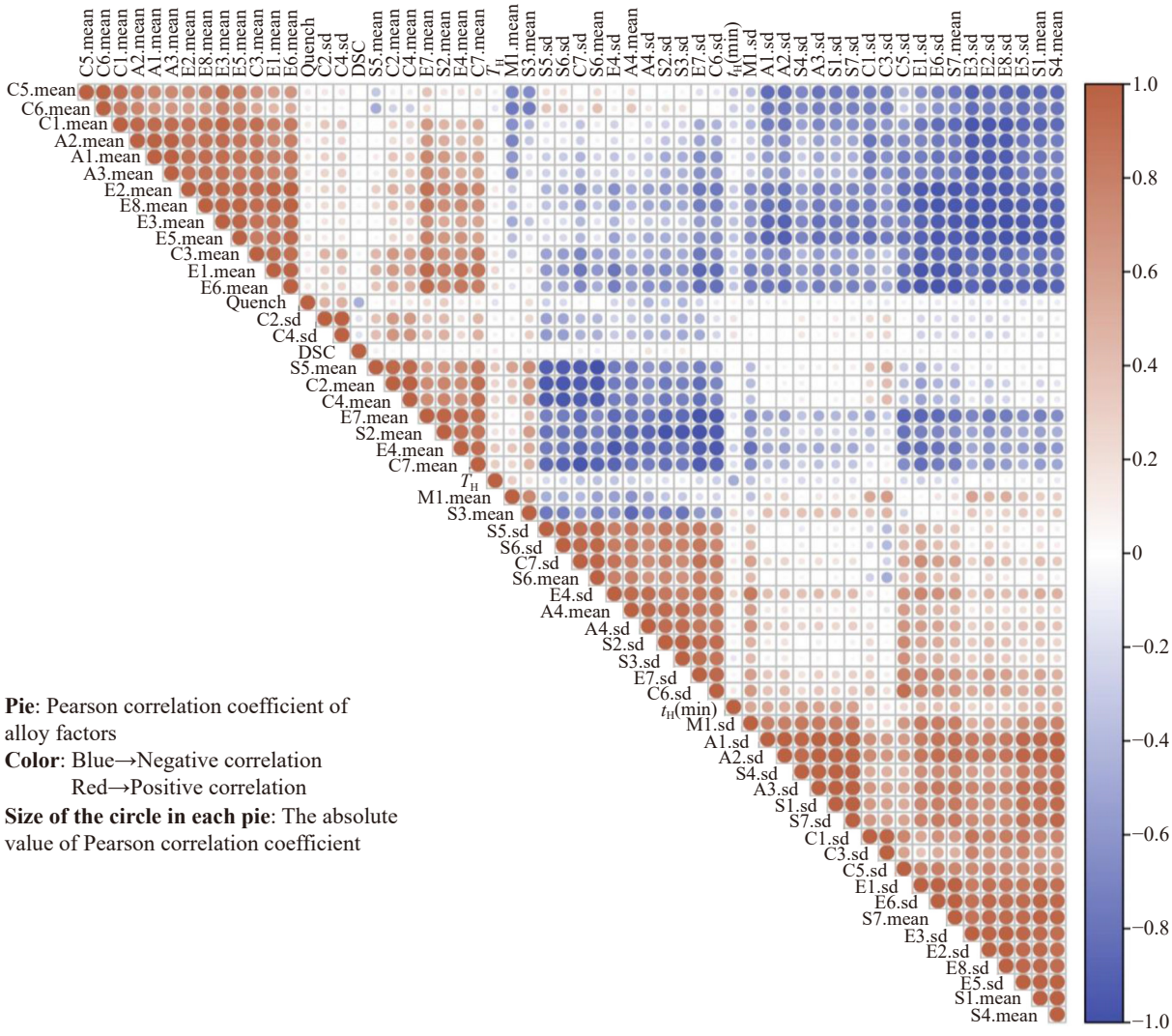

Fig. 3. Correlation coefficient of correlation screening process for 58 alloy factors.

factors related to transformation temperature (M_f, M_s, A_s, and A_f) were obtained.

Fig. 4 shows the results of the recursive elimination of the alloying factors associated with the transformation temperature (M_f, M_s, A_s, and A_f). With the continuous reduction of recursively eliminated features, the error of the support vector regression model is also gradually reduced, indicating that the eliminated alloy factor contributes little to the model, causing a large error in model training. With the continuous elimination of recursion and the reduction of variable dimensions, the prediction accuracy of the SVR model continues to increase until the remaining alloy factors are reduced to less than 8. The alloy factor eliminated later contains important information and plays an important role in improving the prediction accuracy of the model. At this point, the recursive elimination screening process is completed. After recursive elimination, there are 5 main alloying factors affecting M_f and M_s, and the corresponding model errors are 2.32% and 1.64%, respectively. There are 7 main alloying factors affecting A_s, and the model error is 2.06%. There are 6 main alloy factors affecting A_f, and the model error is 1.86%. These main alloying factors are related to lattice constant, atomic mass, ionization energy, atomization enthalpy, vacancy enthalpy change, melting point, electron size, Mendeleev number, bulk modulus, and stiffness modulus etc.

Fig. 5 shows the results of exhaustive screening of alloy factors related to transformation temperature (M_f, M_s, A_s, and A_f). Many combinations of 2–7 principal alloying factors result in the same minimum error level. The results show that the exhaustive method can effectively reduce the variable dimension and improve the design efficiency. The M_f model has the smallest correlation error of 2.15% with the combination of E5.sd, C1.sd, and M1.sd, and the correlation error of M_s model is the smallest, which is 1.77% for the combination of A3.sd, E3.sd, C2.sd, M1.sd, and S6.sd, the smallest correlation error of A_s model, which is 1.80% can be achieved for the combination of C3.mean, S2.sd, and Quench, and the smallest error of A_f model of 1.83% can be obtained with the combination of C3.mean, C3.sd, and S6.sd. Therefore, E5.sd, C1.sd, M1.sd, A3.sd, E3.sd, C2.sd, M1.sd, S6.sd, C3.mean, C3.sd, S2.sd, and Quench are called key alloying factors, and the corresponding element characteristics of the 11 factor combinations are listed in Table 2.

In addition, the interpretable model SHAP for visual analysis was employed to better express the primary and secondary factors affecting material phase transitions, as shown in

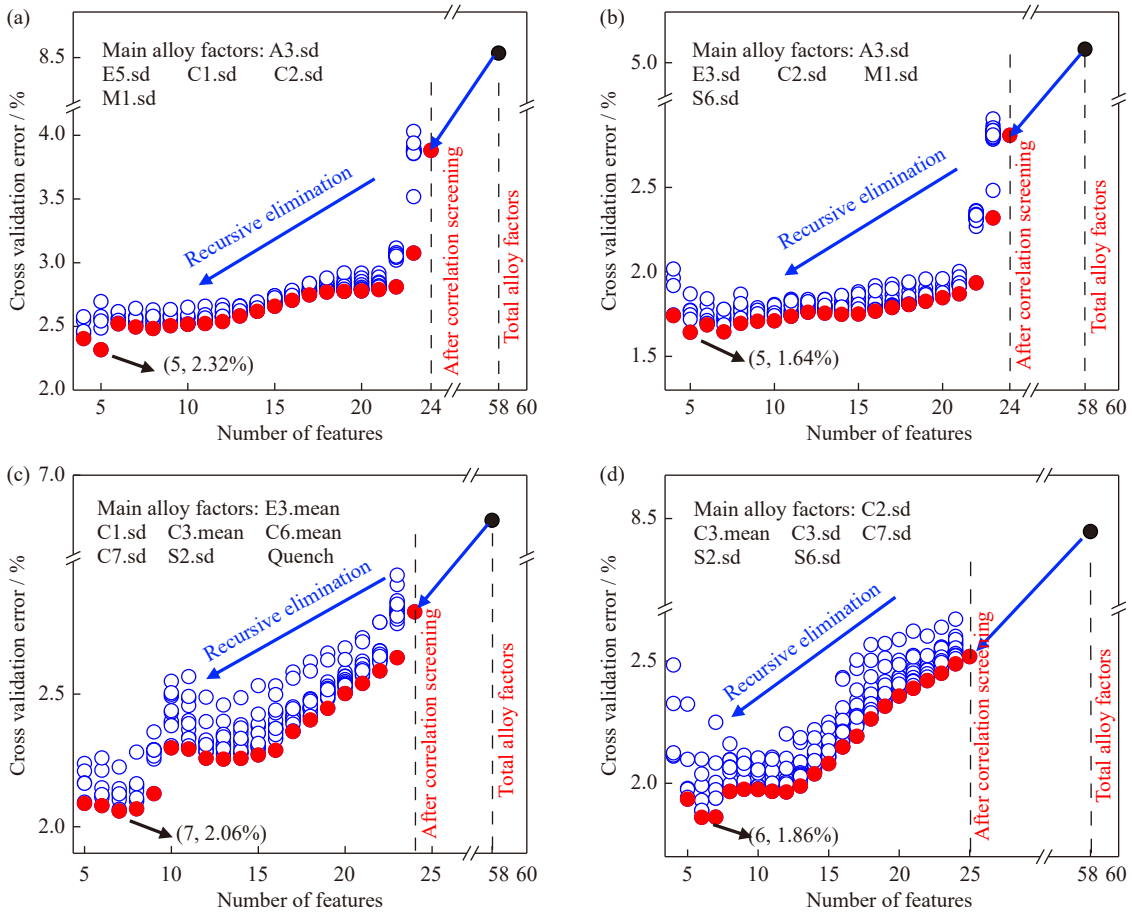

Fig. 4. Recursive elimination process: (a) M_f recursive elimination; (b) M_s recursive elimination; (c) A_s recursive elimination; (d) A_f recursive elimination. Each dot indicates a combination of alloy factors and the solid dots are the combinations with minimum model error under the number of alloy factors after elimination.

Fig. 6. The average absolute values of SHAP scores for key factors influence the phase transition point. Among them, the average absolute SHAP values for the key factors affecting the phase transition point M_f, namely E5.sd, C1.sd, and M1.sd, are 26.52, 36.64, and 31.68, respectively. From the data, it can be observed that among these three key factors, C1.sd has the most significant impact on the M_f phase transition, followed by M1.sd, and lastly, E5.sd. For the phase transition point M_s, the average absolute SHAP values for the key factors A3.sd, E3.sd, C2.sd, M1.sd, and S6.sd are 9.09, 15.13, 19.86, 13.65, and 35.85, respectively. Hence, it can be concluded that the most influential factors on the M_s phase transition are ranked from highest to lowest impact as follows: S6.sd, C2.sd, E3.sd, M1.sd, and A3.sd. Regarding the phase transition point A_s, the average absolute SHAP values for the key factors C3.mean, S2.sd, and Quench are 35.29, 58.38, and 33.32, respectively. Therefore, it is evident that the most significant factor influencing the A_s phase transition is S2.sd, followed by C3.mean, and Quench. Finally, for the phase transition point A_f, the average absolute SHAP values for the key factors C3.mean, C3.sd, and S6.sd are 26.51, 42.93, and 38.28, respectively. Among these factors, C3.sd has the most substantial impact on the A_f phase transition, followed by S6.sd, while C3.mean has the least impact.

On the above basis, four effective alloy performance prediction models were established, including M_f prediction model with E5.sd, C1.sd, and M1.sd as input, M_s prediction model with A3.sd, E3.sd, C2.sd, M1.sd, and S6.sd as input, A_s prediction model with C3.mean, S2.sd, and Quench as input, and A_f prediction model with C3.mean, C3.sd, and S6.sd as input. The predicted properties of the four models and the corresponding experimentally measured properties are shown in Fig. 7. The results show that all the four models of M_f, M_s, A_s, and A_f have satisfactory prediction accuracy, the prediction error of the M_f model, M_s model, A_s model, and A_f model is less than 1.7%, 0.8%, 1.5%, and 1.7%, respectively.

As shown in Table 3, comparing the prediction results of the two modeling methods, feature modeling has smaller prediction errors and higher accuracy than component modeling. The difference in accuracy than component modeling. The difference in accuracy between the feature modeling training set and the testing set is small, resulting in better fitting results. The component direct modeling contains too much redundant information, resulting in relatively low accuracy in predicting phase transition temperature, while feature screening has removed features that have a small impact on phase transition temperature, obtaining key features that can reasonably construct the model, thereby improving model accuracy.

To verify the accuracy of the model prediction, a group of alloy compositions ($Cu_{80.52}Al_{8.68}Mn_{10.8}$, wt%) with the room temperature phase transition temperature was selected in the

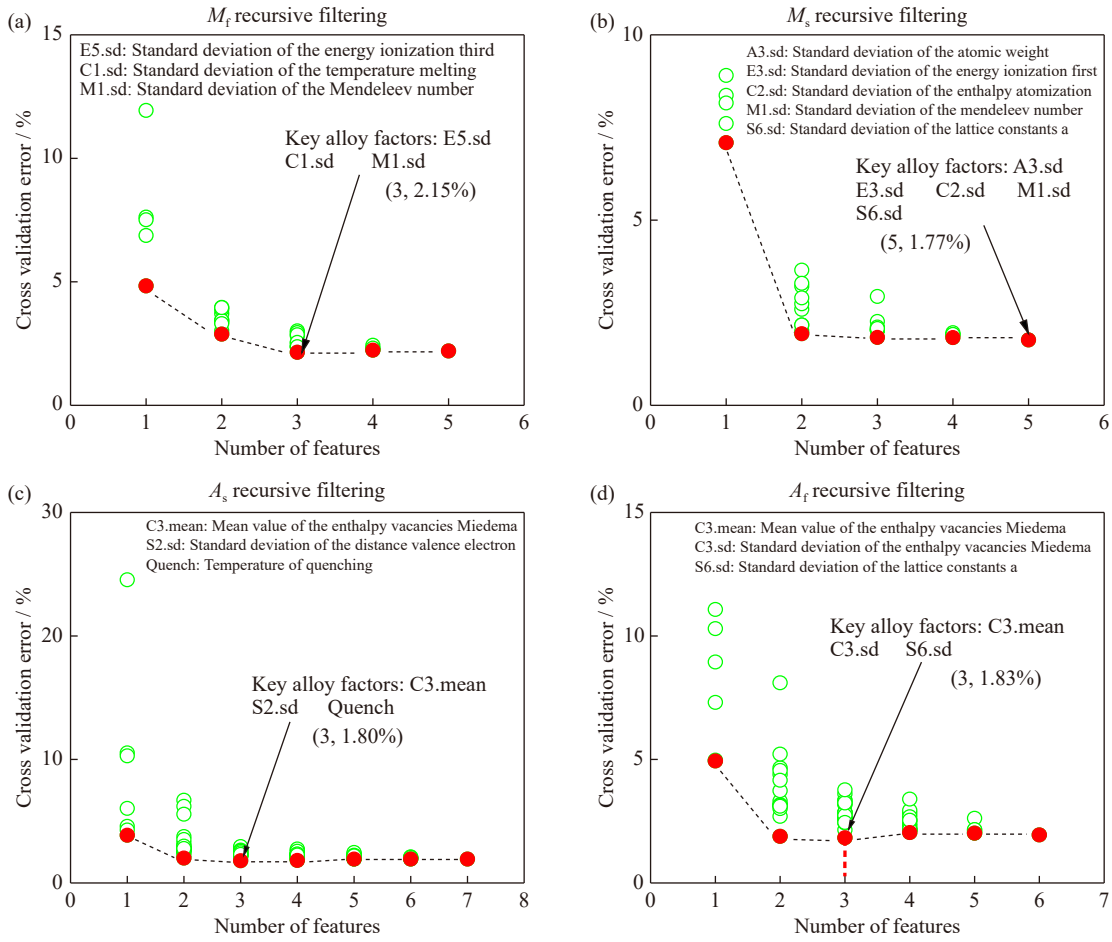

Fig. 5. Exhaustive screening process: (a) M_f exhaustive screening; (b) M_s exhaustive screening; (c) A_s exhaustive screening; (d) A_f exhaustive screening.

Table 2. Key alloying factors obtained by exhaustive screening

Main alloy factors affecting M_f		Main alloy factors affecting M_s		Main alloy factors affecting A_s		Main alloy factors affecting A_f	
Factors	Description	Factors	Description	Factors	Description	Factors	Description
E5.sd	Standard deviation of the third ionization energy	C2.sd	Standard deviation of the enthalpy of atomization	Quench	Quenching temperature	C3.sd	Standard deviation of the vacancy enthalpy change
M1.sd	Standard deviation of the Mendeleev number	A3.sd	Standard deviation of the atomic mass	C3.mean	The vacancy enthalpy change	C3.mean	The vacancy enthalpy change
C1.sd	Standard deviation of the melting point	E3.sd	Standard deviation of the first ionization energy	S2.sd	Standard deviation of the valence electron distance	S6.sd	Standard deviation of the lattice constant
—	—	M1.sd	Standard deviation of the Mendeleev number	—	—	—	—
—	—	S6.sd	Standard deviation of the lattice constant	—	—	—	—

unexplored range. The phase transition temperature of the alloy was obtained by DSC test, and compared with the results of component modeling and feature modeling. The experimental results were found to be in good agreement with the predictions of the ML model, suggesting that ML can enable efficient design of SMAs (Table 4).

4. Discussion

Compared with the element feature modeling process, the composition modeling is simple and does not require domain knowledge, experience, and the process of element feature extraction and screening [48]. However, the composition modeling contains too much redundant information [37,49], resulting in slightly lower alloy prediction accuracy than feature modeling (Table 4). Feature modeling can establish accurate models even when the amount of data is small, and the model has a certain degree of generalization ability [37]. However, feature modeling requires feature extraction and screening, with complex processes and high equipment re-

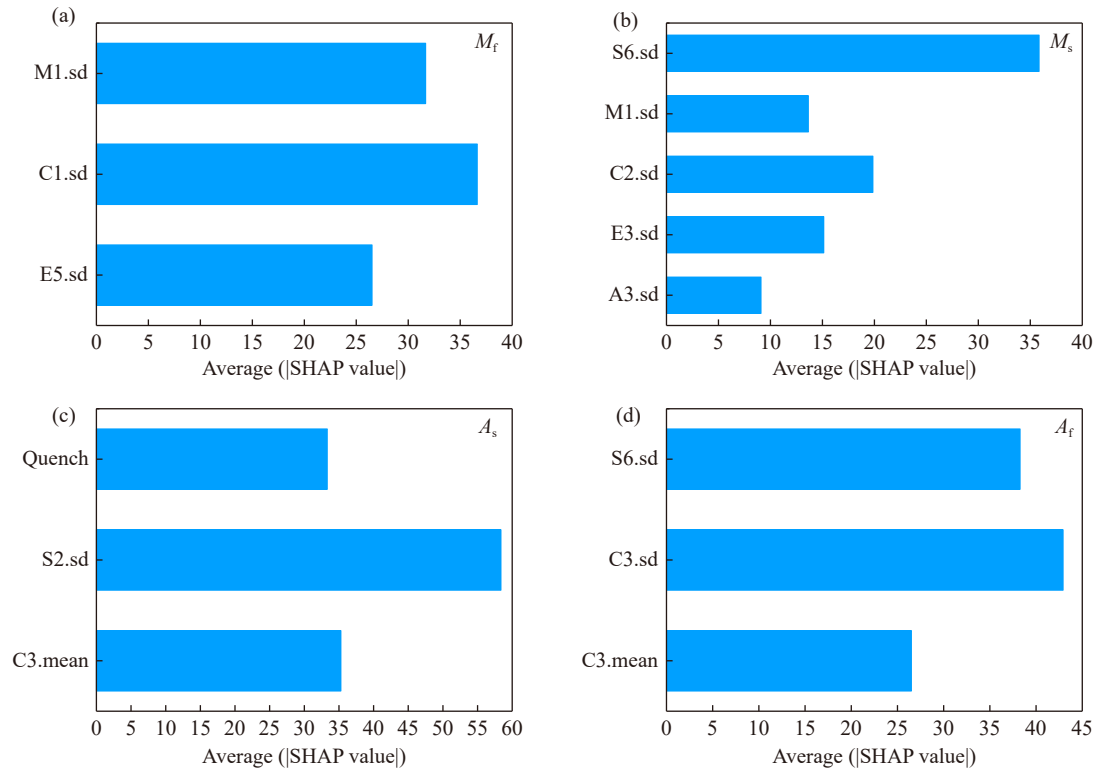

Fig. 6. Average of SHAP values for key factors influence the phase transition point: (a) M_f model; (b) M_s model; (c) A_s model; (d) A_f model.

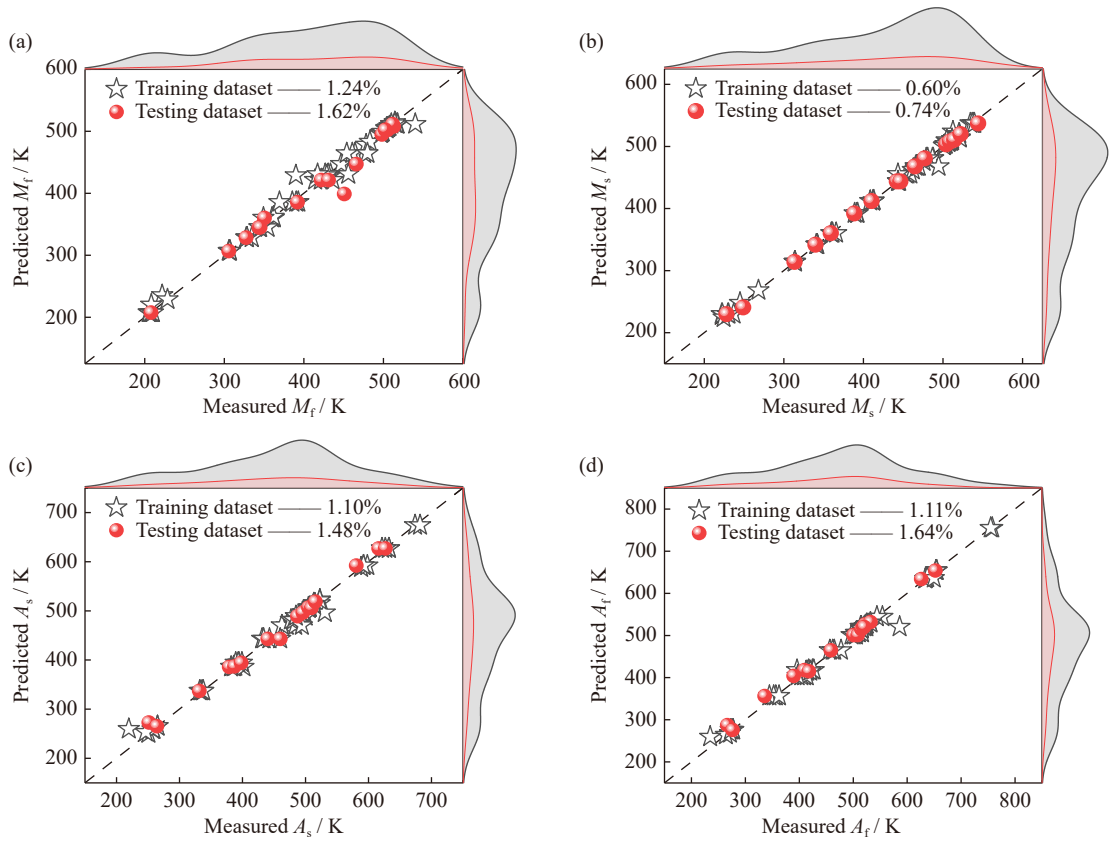

Fig. 7. Prediction results of feature modeling with the key alloy factors as inputs: (a) predict error of M_f model; (b) predict error of M_s model; (c) predict error of A_s model; (d) predict error of A_f model. The shaded areas represent data distribution plots for the X and Y axes, offering a more convenient and visual depiction of the data distribution on both axes.

quirements [50]. In addition, using features for modeling can not only avoid the influence of components on the prediction model, but also clarify the relationship between performance and features. Therefore, feature modeling can be used to bet-

Table 3. Comparison of prediction results between component modeling and feature modeling

Phase transition temperature / K	Prediction error of component modeling			Prediction error of feature modeling		
	Training dataset / %	Testing dataset / %	Δerror / %	Training dataset / %	Testing dataset / %	Δerror / %
M_f	1.90	3.41	1.51	1.24	1.62	0.38
M_s	1.09	2.57	1.55	0.60	0.74	0.14
A_s	1.97	3.58	1.61	1.10	1.48	0.38
A_f	3.96	4.49	0.53	1.11	1.64	0.53

Table 4. Comparison between modeling prediction results and experimental results

Phase transition temperature / K	Experimental temperature / K	Component modeling		Feature modeling	
		Predicted temperature / K	Prediction error of alloy / %	Predicted temperature / K	Prediction error of alloy / %
M_f	246.96	237.60	–3.79	238.96	–3.24
M_s	251.16	250.31	–0.34	253.49	–0.93
A_s	257.25	262.21	+1.93	257.15	–0.038
A_f	260.64	275.59	+5.74	260.54	–0.038

Notes: A positive error indicates that the predicted value is higher than the measured value, and a negative error indicates that the predicted value is lower than the measured value.

ter show the connection between material properties and characteristics, so as to continuously realize the transition of machine learning from scratch, i.e., transition from black box to gray box, and then to transparent box.

There were many previous studies on phase transition temperature, and researchers have summarized the relationship between phase transition points and alloy compositions [51]. In many empirical formulas, there appears to be a relatively simple linear correlation between the phase transition points of SMAs and their compositions under the same conditions, as shown in Eqs. (5)–(6).

$$M_s = 706 - 32.3\mathrm{Al} - 20.7\mathrm{Fe} + 41.5\mathrm{Mn} - 26.3\mathrm{Ni} \quad (5)$$

$$M_s = 179 + 7.2e_v/a \quad (6)$$

where e_v/a is the valence electron concentration.

The regression analysis statistical data for Eq. (5) were obtained as follows: S = 38.3851; R–Sq = 87.96% and R–Sq(adj) = 81.93%. The regression analysis statistical data for Eq. (6) were obtained as follows: S = 94.2735; R–Sq = 0.11% and R–Sq(adj) = 0.00% [51]. In the regression equation, S represents the sum of squared residuals, which is used to measure the degree of fit of the model and the magnitude of prediction errors. The smaller the sum of squared residuals for a set of data, the better the fit. R–Sq, or the coefficient of determination, is an indicator used to measure how well the regression model fits the observed data. An R–Sq close to 1 indicates that the model can explain a significant portion of the variability in the dependent variable, indicating a good fit. On the other hand, an R–Sq close to 0 suggests that the model fails to effectively explain the variability in the dependent variable, indicating a poor fit. R–Sq(adj), known as the adjusted coefficient of determination, is a correction to R–Sq designed to more accurately reflect the model's fit. A higher R–Sq(adj) value, closer to 1, indicates a better fit of the model to the observed data.

However, using this simple linear empirical formula to predict the alloy's phase transition may result in significant errors, as shown in Table 5.

The average prediction error of empirical equations is 17.91%. By comparing the two methods, it can be observed that the accuracy of machine learning predictions for phase transition points is significantly higher than that of empirical formulas. Moreover, empirical formulas mainly focus on predicting the M_s point, while the machine learning approach in this paper predicts all four phase transition points of SMAs.

It is well known that the martensitic phase transformation of alloys is produced by the shear displacement of atoms in the alloy, accompanied by the breaking and bonding of atomic bonds. Therefore, the difficulty of martensitic transformation essentially depends on the strength of the bond between

Table 5. Error for predicting alloy phase transition temperatures using empirical equation [51]

Alloy composition / wt%	Experimental value of M_s / K	Equation predicted value of M_s / K	Prediction error / %
$Cu_{85.19}Al_{10.21}Fe_{4.6}$	581	553.997	4.65
$Cu_{84.41}Al_{11.17}Fe_{4.42}$	528	526.715	0.24
$Cu_{83.86}Al_{11.56}Fe_{4.58}$	505	510.806	1.15
$Cu_{83.47}Al_{11.91}Fe_{4.62}$	476	498.673	4.76
$Cu_{84.83}Al_{12.57}Fe_{2.6}$	539	519.169	3.68
$Cu_{86.1}Al_{12.58}Fe_{1.32}$	523	545.342	4.27
$Cu_{85.29}Al_{12.6}Fe_{2.11}$	532	528.343	0.69
$Cu_{83.05}Al_{12.6}Fe_{4.35}$	408	481.975	18.13
$Cu_{82.77}Al_{12.96}Ni_{4.27}$	422	448.091	6.18
$Cu_{83.6}Al_{13.15}Ni_{3.25}$	410	468.78	14.34
$Cu_{82.5}Al_{13.5}Ni_4$	335	437.75	30.67
$Cu_{82.3}Al_{13.7}Ni_4$	301	431.29	43.29
$Cu_{82.2}Al_{13.8}Ni_4$	284	428.06	50.73
$Cu_{82}Al_{14}Ni_4$	251	421.6	67.97

atoms, while the strength of the atomic bond is closely related to the valence electrons in the atom.

Ionization energy (I) refers to the energy required for electrons to move from atoms to vacuum when alloy atoms lose electrons [52–54]. The higher the third ionization energy of the element, the more energy is required for the martensitic transformation to occur, and the lower the martensitic transformation finish temperature M_f is. The smaller the standard deviation factor E5.sd of the third ionization energy of the alloy is, the closer the third ionization energy of each element in the alloy is, and the ability of atoms to provide electrons is similar, the lower the martensitic phase transition finish temperature M_f.

The melting point of the alloy represents the bonding strength between the atoms of the alloy [53]. A high melting point indicates that the bonding between atoms is strong, and the more energy required for atoms to undergo shear transformation, the less likely it is to undergo phase transformation, thus requiring more heat energy to promote phase transformation. Therefore, the finish temperature of the martensitic transformation corresponding to the alloy is higher. The smaller the melting point standard deviation C1.sd is, the smaller the melting point difference of each alloy element is, the smaller the bonding force between atoms is, correspondingly, the relatively lower melting point and lower martensitic transformation finish temperature M_f the obtained alloy has, and vice versa.

The Mendeleev number (M1) of an element is defined by the Pauling electronegativity χ and atomic radius R_a of the element at any pressure, that is, the regression line of the Pauling electronegativity χ and atomic radius R_a in 2D space projects the element sequence number [27,53]. Among them, the Pauling electronegativity χ is the scale of the ability of two different element atoms to attract electrons when they form a chemical bond in a compound, which can be estimated by ionization energy and electron affinity, that is, the average value of ionization energy (I) and electron affinity energy (A) [55].

$$\chi = \frac{1}{2}(|I| + |A|) \tag{7}$$

where I is the ionization energy, which is the energy required to move electrons from the atom to the vacuum, A is the electron affinity energy, which is the energy released by the atom when it gets an electron. The greater the electronegativity value of an element, the more energy the atom needs/releases to lose/gain electrons, and the ability of its atoms to provide/attract electrons in the alloy is weak, that is, when different element atoms form an alloy, the atom contributes little to the free electron density and requires less external energy, and the phase transition temperature is low. Besides, the atomic radius is related to two factors, the electron configuration outside the nucleus and the number of nuclear charges. That is, when the atomic radius is small, the number of electron shells is small or the number of nuclear charges is large. This situation leads to a large attraction of the nucleus to the electrons outside the nucleus, so that the atom needs more energy to form an alloy with other atoms, and the phase transition temperature is high.

The atomic mass of an atom can also be used for evaluating the valence electrons of an element. The larger the standard deviation A3.sd of the atomic mass of the element is, the stronger the ability of each atom to gain or lose electrons, the greater the bonding strength between the formed alloy atoms, and the greater the resistance of the alloy to martensitic phase transformation, resulting in higher martensitic phase transition temperature, and vice versa. The larger the atomic radius, the larger the atomic bond length, the smaller the bond energy, and the easier it is to lose electrons. The less energy required for alloy phase transformation, the lower the martensitic transformation temperature.

The enthalpy of atomization is the change in enthalpy of an elemental gas atom that produces 1 mole of the elemental substance. The metal element has low atomization enthalpy and ionization energy, and the melting point of the alloy is low. For elemental metals, the smaller the atomization enthalpy of elements is, the smaller the strength of metal bonds between atoms is, the smaller the energy required for metal phase transformation is, and the less external heat is required for phase transformation, so the alloy phase transformation temperature is relatively lower, that is, the martensitic transformation start temperature M_s is lower. It can be proposed that the larger the standard deviation of the atomic enthalpy of each element in the alloy is, the greater the fluctuation of the atomic enthalpy of each element in the alloy is, and the greater the metal bonding energy between atoms is. The more energy required for the phase transformation of the alloy, the greater the temperature difference required for the phase transformation of the alloy, and the higher the martensitic transformation start temperature M_s.

The lattice constant a represents the side length of a single unit cell in the alloy. In general (with a special note that this does not apply to porous materials and isotopically labeled crystalline materials), the distance between atoms in a metal is proportional to the lattice constant a. The larger the lattice constant a, the lower lattice density, the greater the distance between atoms, the weaker the bonding force between atoms, and less energy is required for phase transition. At this time, only a low temperature difference is required to complete the martensitic transformation, resulting in a relatively low martensitic transformation start temperature M_s. The smaller the standard deviation of the lattice constant a of alloy atoms, the closer the atomic distance of each element in the alloy is to the average value of the atomic distance. In this case, the bonding energy between the atoms of the alloy formed is small, resulting in a smaller driving force required for the alloy phase transformation, so that the martensitic transformation start temperature M_s is low.

The vacancy formation is due to the thermal movement of the atom, which makes the energy of an atom high enough to overcome the energy barrier to break the bonds between an atom inside the crystal and its nearest neighbor atoms, and the atom leaves its equilibrium position. The formation of va-

cancies causes lattice distortion, accompanied by the breaking of atomic bonds. Therefore, the formation of vacancies requires energy, that is, vacancy formation energy. The martensitic transformation is carried out in the form of atomic shear, accompanied by the continuous generation of vacancies. The vacancy enthalpy change is the enthalpy change value generated when vacancies are formed in the alloy, and it is proportional to the vacancy formation energy. The greater the enthalpy change of vacancies, the more energy is required to form vacancies, and thus the greater the thermal energy difference required for the alloy phase transition, the higher the alloy phase transition temperature.

The valence electron distance is the distance from the valence electrons of an atom to the nucleus [56]. The greater the distance between the valence electrons of atoms, the greater the bonding force between atoms, the more energy required for phase transformation, and the higher the austenite transformation start temperature A_s, and vice versa. The larger the standard deviation S2.sd of the atomic valence electron distance, the stronger the ability of each atom to lose or gain electrons, and the greater the interaction force between atoms after forming an alloy. Correspondingly, more energy is required for alloy atomic shear, and the austenite transformation start temperature A_s of the alloy is higher.

The quenching temperature directly affects the phase transformation process and structure of the alloy, thereby affecting the phase transformation temperature of the alloy. For CuAlNi alloy, the phase transition temperature decreases first and then increases with the increase of quenching temperature; while for NiTiNb alloy, the higher the quenching temperature, the higher the phase transition temperature. This indicates that the quenching temperature has a great influence on the phase transition temperature of the alloy.

Through the interpretable model's SHAP visualization analysis of individual prediction points (Fig. 8), the more intuitive understanding of the impact of key factors on the distribution of material phase transition points for each data point was obtained. From Fig. 8(a), the SHAP value distribution of C1.sd is predominantly concentrated within the range of less than –20 and greater than or equal to 40. In contrast, E5.sd's SHAP values are mostly distributed within the range of 0 to 40, while M1.sd's SHAP values exhibit a relatively uniform distribution. Consequently, C1.sd yields the highest average absolute SHAP value, signifying its most substantial contribution to the model. Hence, C1.sd is identified as the foremost key factor influencing M_f. Similarly, as observed from Fig. 8(b), the SHAP values of S6.sd for each data point are primarily situated at higher values, underscoring S6.sd's substantial contribution to the M_s model and, by extension, establishing it as the most pivotal key factor influencing M_s. The remaining four key factors predominantly exhibit SHAP value distributions within lower ranges, suggesting relatively minor contributions to the M_s model. In Fig. 8(c), the SHAP values of S2.sd for each data point exhibit some elevated values, indicating that specific S2.sd values exert a noteworthy influence on the A_s model's output. This ultimately designates S2.sd as the most significant key factor impacting A_s, with an impressively high average SHAP absolute value of 53.38. Conversely, C3.mean and Quench predominantly manifest SHAP values within lower value ranges, thereby signifying a secondary impact on A_s. Fig. 8(d) illustrates that C3.sd possesses some prominent SHAP values, leading to its highest average value. Consequently, C3.sd contributes more significantly to the A_f model than the other two factors, emerging as the preeminent factor influencing A_f.

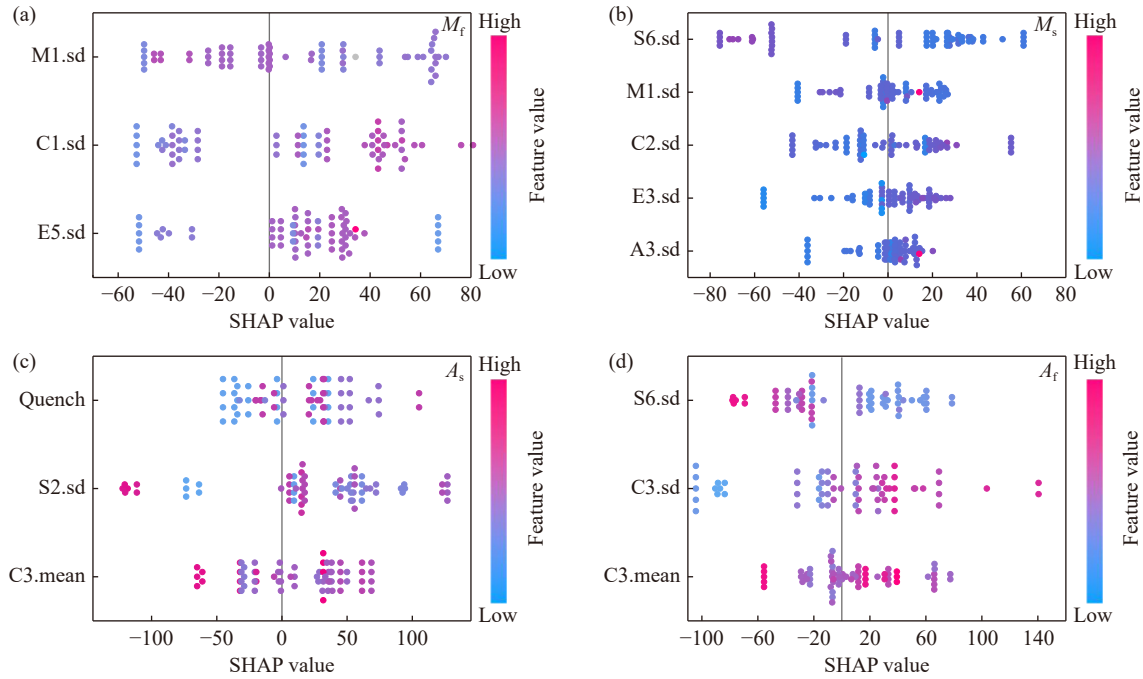

Fig. 8. SHAP value representing the influence of key factors on phase transition points for each data point: (a) M_f model; (b) M_s model; (c) A_s model; (d) A_f model.

5. Conclusions

The phase transition temperature of Cu-based shape memory alloys has been successfully predicted by composition modeling and element feature modeling. Both models have achieved satisfactory prediction accuracy, the prediction accuracy of the composition model has reached more than 95.5%, and the prediction accuracy of the element feature model is over 98.3%. The experimental results are consistent with the predictions of the ML model, suggesting that ML is an effective tool for designing SMAs. On the basis of the analysis above, several key features related to phase transition temperature were determined by using this method, and the mechanism of the influence of key features on phase transition temperature was analyzed. This work may provide a new understanding of the factors that affecting phase transformation temperature and guide the efficiently design of Cu-based shape memory alloys according to the material application temperature domain.

Acknowledgements

This work is financially supported by the National Natural Science Foundation of China (No. 51974028).

Conflict of Interest

The authors declare that they have no competing financial interests or personal relationships that may have influenced the work reported in this study.

References

[1] H.Y. Wang, D. Xu, J.C. Feng, S. Chao, and H. Sun, Shape memory properties of additive manufacturing Cu–Al–Mn–Ni alloys with different Ni contents, *MRS Commun.*, 13(2023), No. 3, p. 526.

[2] Y.K. Zhang, L.Y. Xu, L. Zhao, *et al*., Process-microstructure-properties of CuAlNi shape memory alloys fabricated by laser powder bed fusion, *J. Mater. Sci. Technol.*, 152(2023), p. 1.

[3] C.Y. Xiong, Y. Li, J. Zhang, *et al*., Superelasticity over a wide temperature range in metastable β-Ti shape memory alloys, *J. Alloys Compd.*, 853(2021), art. No. 157090.

[4] Q.K. Meng, J.D. Xu, H. Li, *et al*., Phase transformations and mechanical properties of a $Ti_{36}Nb_5Zr$ alloy subjected to thermo-mechanical treatments, *Rare Met.*, 41(2022), No. 1, p. 209.

[5] Y.H. Sun, Y. Zhao, Y.Y. Zhao, *et al*., Improving exposure of anodically ordered Ni–Ti–O and corrosion resistance and biological properties of NiTi alloys by substrate electropolishing, *Rare Met.*, 40(2021), No. 12, p. 3575.

[6] R. Yang, S. Li, N. Zhang, C. Wang, T.M. Wang, and Q.H. Wang, Tribology behaviors of Ti–$Ni_{51.5}$at% shape memory alloy with different microstructures and textures, *Rare Met.*, 40(2021), No. 12, p. 3616.

[7] X. Feng, L.M. Zhao, X.J. Mi, *et al*., Improving interface adhesion in TiNi wire/shape memory epoxy composites using carbon nanotubes, *Rare Met.*, 40(2021), No. 4, p. 934.

[8] M.W. Wu, Y. Xiao, Z.F. Hu, R.P. Liu, and C.M. Ma, Enhanced superelasticity of Cu–Al–Ni shape memory alloys with strong orientation prepared by horizontal continuous casting, *Front. Mater. Sci.*, 16(2022), No. 4, art. No. 220616.

[9] P. Motzki and S. Seelecke, *Encyclopedia Smart Materials*. Elsevier, Amsterdam, 2022, p. 254.

[10] Y. Wang, J. Venezuela, and M. Dargusch, Biodegradable shape memory alloys: Progress and prospects, *Biomaterials*, 279(2021), art. No. 121215.

[11] N. Gangil, A.N. Siddiquee, and S. Maheshwari, Towards applications, processing and advancements in shape memory alloy and its composites, *J. Manuf. Process.*, 59(2020), p. 205.

[12] N.A. Hamid, A. Ibrahim, and A. Adnan, Smart structures with Pseudoelastic and Pseudoplastic shape memory alloy: A critical review of their prospective, feasibility and current trends, *IOP Conf. Ser.*, 469(2019), art. No. 012123.

[13] S. Santosh, J. Kevin Thomas, K. Rajkumar, and A. Sabareesh, Effect of Ni and Mn additions on the damping characteristics of Cu–Al–Fe based high temperature shape memory alloys, *J. Alloys Compd.*, 924(2022), art. No. 166258.

[14] T.N. Raju and V. Sampath, Influence of aluminium and iron contents on the transformation temperatures of Cu–Al–Fe shape memory alloys, *Trans. Indian Inst. Met.*, 64(2011), No. 1, art. No. 165.

[15] Y. Sutou, R. Kainuma, and K. Ishida, Effect of alloying elements on the shape memory properties of ductile Cu–Al–Mn alloys, *Mater. Sci. Eng. A*, 273-275(1999), p. 375.

[16] R. Dasgupta, A.K. Jain, P. Kumar, S. Hussain, and A. Pandey, Role of alloying additions on the properties of Cu–Al–Mn shape memory alloys, *J. Alloys Compd.*, 620(2015), p. 60.

[17] S.U. Rehman, M. Khan, A.N. Khan, *et al*., Influence of Cu addition on transformation temperatures and thermal stability of Ti-NiPd high temperature shape memory alloys, *Proc. Inst. Mech. Eng.*, 233(2019), No. 5, p. 800.

[18] I.N. Qader, E. Öner, M. Kok, *et al*., Mechanical and thermal behavior of $Cu_{84-x}Al_{13}Ni_3Hf_x$ shape memory alloys, *Iran. J. Sci. Technol. Trans. A*, 45(2021), No. 1, p. 343.

[19] K.K. Alaneme, E.A. Okotete, and J.U. Anaele, Structural vibration mitigation–A concise review of the capabilities and applications of Cu and Fe based shape memory alloys in civil structures, *J. Build. Eng.*, 22(2019), p. 22.

[20] M.H.S. Segler, M. Preuss, and M.P. Waller, Planning chemical syntheses with deep neural networks and symbolic AI, *Nature*, 555(2018), No. 7698, p. 604.

[21] X.J. Wang, S. Ye, W. Hu, *et al*., Electric dipole descriptor for machine learning prediction of catalyst surface–molecular adsorbate interactions, *J. Am. Chem. Soc.*, 142(2020), No. 17, p. 7737.

[22] Z.H. Lian, M.J. Li, and W.C. Lu, Fatigue life prediction of aluminum alloy via knowledge-based machine learning, *Int. J. Fatigue*, 157(2022), art. No. 106716.

[23] R. Jaafreh, U.M. Chaudry, K. Hamad, and T. Abuhmed, Age-hardening behavior guided by the multi-objective evolutionary algorithm and machine learning, *J. Alloys Compd.*, 893(2022), art. No. 162104.

[24] J. Wei, X. Chu, X.Y. Sun, *et al*., Machine learning in materials science, *InfoMat*, 1(2019), No. 3, p. 338.

[25] L. Qiao, Y. Liu, and J.C. Zhu, A focused review on machine learning aided high-throughput methods in high entropy alloy, *J. Alloys Compd.*, 877(2021), art. No. 160295.

[26] N. Qu, Y. Liu, Y. Zhang, *et al*., Machine learning guided phase formation prediction of high entropy alloys, *Mater. Today Commun.*, 32(2022), art. No. 104146.

[27] Y. Zhang, C. Wen, C.X. Wang, *et al*., Phase prediction in high entropy alloys with a rational selection of materials descriptors and machine learning models, *Acta Mater.*, 185(2020), p. 528.

[28] D.Z. Xue, P.V. Balachandran, J. Hogden, J. Theiler, D.Q. Xue, and T. Lookman, Accelerated search for materials with targeted properties by adaptive design, *Nat. Commun.*, 7(2016), art. No. 11241.

[29] D.Z. Xue, D.Q. Xue, R.H. Yuan, *et al*., An informatics approach to transformation temperatures of NiTi-based shape memory alloys, *Acta Mater.*, 125(2017), p. 532.
[30] C. Wen, Y. Zhang, C.X. Wang, *et al*., Machine learning assisted design of high entropy alloys with desired property, *Acta Mater.*, 170(2019), p. 109.
[31] C. Wen, C.X. Wang, Y. Zhang, *et al*., Modeling solid solution strengthening in high entropy alloys using machine learning, *Acta Mater.*, 212(2021), art. No. 116917.
[32] K. Kaufmann and K.S. Vecchio, Searching for high entropy alloys: A machine learning approach, *Acta Mater.*, 198(2020), p. 178.
[33] Z.Q. Zhou, Y.J. Zhou, Q.F. He, Z.Y. Ding, F.C. Li, and Y. Yang, Machine learning guided appraisal and exploration of phase design for high entropy alloys, *NPJ Comput. Mater.*, 5(2019), art. No. 128.
[34] K. Lee, M.V. Ayyasamy, P. Delsa, T.Q. Hartnett, and P.V. Balachandran, Phase classification of multi-principal element alloys via interpretable machine learning, *NPJ Comput. Mater.*, 8(2022), art. No. 25.
[35] Y.F. Ye, Q. Wang, J. Lu, C.T. Liu, and Y. Yang, High-entropy alloy: Challenges and prospects, *Mater. Today*, 19(2016), No. 6, p. 349.
[36] F. Yang, Z. Li, Q. Wang, *et al*., Cluster-formula-embedded machine learning for design of multicomponent β-Ti alloys with low Young's modulus, *NPJ Comput. Mater.*, 6(2020), art. No. 101.
[37] X.J. Liu, P.C. Xu, J.J. Zhao, W.C. Lu, M.J. Li, and G. Wang, Material machine learning for alloys: Applications, challenges and perspectives, *J. Alloys Compd.*, 921(2022), art. No. 165984.
[38] C.T. Wu, H.T. Chang, C.Y. Wu, *et al*., Machine learning recommends affordable new Ti alloy with bone-like modulus, *Mater. Today*, 34(2020), p. 41.
[39] H.T. Zhang, H.D. Fu, X.Q. He, *et al*., Dramatically enhanced combination of ultimate tensile strength and electric conductivity of alloys via machine learning screening, *Acta Mater.*, 200(2020), p. 803.
[40] H.T. Zhang, H.D. Fu, S.C. Zhu, W. Yong, and J.X. Xie, Machine learning assisted composition effective design for precipitation strengthened copper alloys, *Acta Mater.*, 215(2021), art. No. 117118.
[41] C.S. Wang, H.D. Fu, L. Jiang, D.Z. Xue, and J.X. Xie, A property-oriented design strategy for high performance copper alloys via machine learning, *NPJ Comput. Mater.*, 5(2019), art. No. 87.
[42] D.F. Tu, J.Q. Yan, Y.B. Xie, *et al*., Accelerated design for magnetocaloric performance in Mn–Fe–P–Si compounds using machine learning, *J. Mater. Sci. Technol.*, 96(2022), p. 241.
[43] M. Rahaman, W.Z. Mu, J. Odqvist, and P. Hedström, Machine learning to predict the martensite start temperature in steels, *Metall. Mater. Trans. A*, 50(2019), No. 5, p. 2081.
[44] I. Guyon, J. Weston, S. Barnhill, and V. Vapnik, Gene selection for cancer classification using support vector machines, *Mach. Learn.*, 46(2002), No. 1-3, p. 389.
[45] L.P. Wang, Y.L. Wang, and Q. Chang, Feature selection methods for big data bioinformatics: A survey from the search perspective, *Methods*, 111(2016), p. 21.
[46] R.H. Yuan, Z. Liu, P.V. Balachandran, *et al*., Accelerated discovery of large electrostrains in $BaTiO_3$-based piezoelectrics using active learning, *Adv. Mater.*, 30(2018), No. 7, art. No. 1702884.
[47] S.J. An, W.Q. Liu, and S. Venkatesh, Fast cross-validation algorithms for least squares support vector machine and kernel ridge regression, *Pattern Recognit.*, 40(2007), No. 8, p. 2154.
[48] Y. Liu, T.L. Zhao, W.W. Ju, and S.Q. Shi, Materials discovery and design using machine learning, *J. Materiomics*, 3(2017), No. 3, p. 159.
[49] K.T. Butler, D.W. Davies, H. Cartwright, O. Isayev, and A. Walsh, Machine learning for molecular and materials science, *Nature*, 559(2018), No. 7715, p. 547.
[50] H.D. Fu, H.T. Zhang, C.S. Wang, W. Yong, and J.X. Xie, Recent progress in the machine learning-assisted rational design of alloys, *Int. J. Miner. Metall. Mater.*, 29(2022), No. 4, p. 635.
[51] V. Sampath, S.V. Gayathri, and R. Srinithi, Experimental and theoretical analyses of transformation temperatures of Cu-based shape memory alloys, *Bull. Mater. Sci.*, 42(2019), No. 5, art. No. 229.
[52] X.H. Li and Z.W. Zhu, Nonlinear dynamic characteristics and stability analysis of energy storage flywheel rotor with shape memory alloy damper, *J. Energy Storage*, 45(2022), art. No. 103392.
[53] P. Villars, K. Brandenburg, M. Berndt, *et al*., Binary, ternary and quaternary compound former/nonformer prediction via Mendeleev number, *J. Alloys Compd.*, 317-318(2001), p. 26.
[54] K. Ciesielski, L.C. Gomes, G.A. Rome, *et al*., Structural defects in compounds ZnXSb (X = Cr, Mn, Fe): Origin of disorder and its relationship with electronic properties, *Phys. Rev. Mater.*, 6(2022), No. 6, art. No. 063602.
[55] R.G. Pearson, Absolute electronegativity and absolute hardness of Lewis acids and bases, *J. Am. Chem. Soc.*, 107(1985), No. 24, p. 6801.
[56] N.J. Sai, P. Rathore, and A. Chauhan, Machine learning-based predictions of fatigue life for multi-principal element alloys, *Scr. Mater.*, 226(2023), art. No. 115214.